Three-Dimensional Structure of RTD-1, a Cyclic Antimicrobial Defensin from Rhesus Macaque Leukocytes[†,‡]

Manuela Trabi,[§,⊥] Horst Joachim Schirra,[§] and David J. Craik*[,§]

Institute for Molecular Bioscience (Centre for Drug Design and Development), University of Queensland, Brisbane, QLD 4072, Australia, and Institute for Biotechnology, Graz University of Technology, A-8010 Graz, Austria

Received August 25, 2000; Revised Manuscript Received January 16, 2001

ABSTRACT: Most mammalian defensins are cationic peptides of 29−42 amino acids long, stabilized by three disulfide bonds. However, recently Tang et al. (1999, *Science 286*, 498−502) reported the isolation of a new defensin type found in the leukocytes of rhesus macaques. In contrast to all the other defensins found so far, rhesus theta defensin-1 (RTD-1) is composed of just 18 amino acids with the backbone cyclized through peptide bonds. Antibacterial activities of both the native cyclic peptide and a linear form were examined, showing that the cyclic form was 3-fold more active than the open chain analogue [Tang et al. (1999) *Science 286*, 498−502]. To elucidate the three-dimensional structure of RTD-1 and its open chain analogue, both peptides were synthesized using solid-phase peptide synthesis and *tert*-butyloxycarbonyl chemistry. The structures of both peptides in aqueous solution were determined from two-dimensional ^{1}H NMR data recorded at 500 and 750 MHz. Structural constraints consisting of interproton distances and dihedral angles were used as input for simulated-annealing calculations and water refinement with the program CNS. RTD-1 and its open chain analogue oRTD-1 adopt very similar structures in water. Both comprise an extended β-hairpin structure with turns at one or both ends. The turns are well defined within themselves and seem to be flexible with respect to the extended regions of the molecules. Although the two strands of the β-sheet are connected by three disulfide bonds, this region displays a degree of flexibility. The structural similarity of RTD-1 and its open chain analogue oRTD-1, as well as their comparable degree of flexibility, support the theory that the additional charges at the termini of the open chain analogue rather than overall differences in structure or flexibility are the cause for oRTD-1's lower antimicrobial activity. In contrast to numerous other antimicrobial peptides, RTD-1 does not display any amphiphilic character, even though surface models of RTD-1 exhibit a certain clustering of positive charges. Some amide protons of RTD-1 that should be solvent-exposed in monomeric β-sheet structures show low-temperature coefficients, suggesting the possible presence of weak intermolecular hydrogen bonds.

Antimicrobial peptides, containing 20−40 amino acid residues, are evolutionarily old elements in host defense mechanisms of various animals and plants. Their active configurations can roughly be divided into α-helical, β-sheet, and mixed structures. Although their general mechanism of action seems to be permeabilizing the cell membrane (*1*−*3*), the significance of their structural variations is still unclear.

Recently, Tang et al. (*4*) reported an α-defensin (named RTD-1) found in rhesus macaque leukocytes that differs from the other defensins discovered so far in sequence, size, and in the fact that its peptide backbone is naturally cyclized. Interestingly, the cyclic RTD-1 peptide shows a 3-fold greater antimicrobial activity than its open chain analogue, oRTD-1. Elucidating the three-dimensional structure of this unusual peptide could help in understanding its mode of action and should bring us one step closer to designing and using such antibiotic peptides for therapeutic applications.

Antimicrobial peptides play an important role in the host defense mechanism of mammals, birds, amphibians, insects, and plants (*5*). Typically, these peptides act on a broad range of microorganisms (Gram-positive and Gram-negative bacteria, fungi, and sometimes even enveloped viruses) to neutralize potentially pathogenic microbes. While the activation of pathogen-specific immune responses occurs relatively slowly, small endogenous antimicrobial peptides are either stored in granules or vesicles, from where they can be excreted quickly, or they can be synthesized rapidly after induction.

Although these antimicrobial peptides all serve the same purpose, their three-dimensional structures are rather diverse. Mammalian defensins are usually folded into β-sheets stabilized by disulfide bonds, whereas insect defensins contain an α-helix linked to a twisted antiparallel β-sheet via disulfide bonds (*6*). Most other antimicrobial peptides, like magainins, cecropins, alamecithin, and melittin, are linear peptides that form an α-helix in the presence of membranes (*3*). Despite these differences in size, sequence, and structure,

[†] This work was supported by the Australian Research Council.

[‡] The coordinates have been deposited (PDB ID 1HVZ, RCSB ID RCSB012617).

* To whom correspondence should be addressed. E-mail: d.craik@imb.uq.edu.au, fax: +61 (7) 3365 2487.

[§] University of Queensland.

[⊥] Graz University of Technology.

10.1021/bi002028t CCC: $20.00
Published on Web 03/16/2001

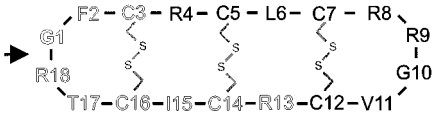

FIGURE 1: Amino acid sequence of RTD-1. The different letter styles indicate the two nona-peptide gene products that make up mature, cyclic RTD-1. The arrow indicates the point where the amide backbone is broken in oRTD-1.

a great number of these peptides exhibit overall dimensions approximating the thickness of a cell membrane, showing one hydrophobic and one hydrophilic face (*2*, *3*).

Defensins were first discovered in the 1960s, when Zeya and Spitznagel (*7*) reported "lysosomal cationic peptides" with antimicrobial properties in rabbit and guinea pig neutrophils. Later, they were also found in humans (*8*), insects (see for example ref *9* and the references therein), and plants (*10*). Defensins comprise 29−42 amino acids, including various cationic residues as well as conserved cysteines. They are divided into two genetically distinct subfamilies (α- and β-defensins) that differ in the number and spacing of conserved residues and in the placement of the cysteines as well as their disulfide connectivity patterns (*11*).

In contrast to the other defensins discovered so far, RTD-1 comprises only 18 amino acids stabilized by three disulfide bonds and has the unusual feature of a cyclic peptide backbone. Several unrelated cyclic tri-disulfide peptides have been isolated from plants of the families Rubiaceae and Violaceae, and they display a broad range of bioactivities. These peptides, referred to as the plant cyclotides (*12*), have a conserved structure in which the six cysteine residues form a cystine knot motif that is embedded in the core of a compact global fold. The plant cyclotides typically contain 29−31 amino acids and are known to be gene products (M. Anderson, D. Craik, C. Jennings, unpublished data). Most other known cyclic peptides are small (<15 amino acids), usually of microbial origin, lack disulfide bonds, and are thought to be nonribosomally synthesized by peptide synthetases. By contrast, RTD-1 is a true gene product that is derived from the posttranslational ligation of two precursor protein fragments. The 20-residue signal peptide and the 44-amino acid prosegment present in each of these two prepropeptides show high sequence similarities to homologous regions of α-defensin precursors (*4*). Nine amino acids of RTD-1 are derived from each of these precursors (indicated in Figure 1), meaning that two ligation reactions have to take place to produce the mature cyclic peptide.

RTD-1 shows antimicrobial activity at micromolar concentrations against both Gram-positive and Gram-negative bacteria as well as fungi (*4*). Interestingly, antibacterial activity of the cyclic peptide was 3-fold greater than that of a tri-disulfide open chain analogue (oRTD-1, see Figure 1), indicating that the cyclic structure is crucial for its bioactivity. In their studies, Tang et al. (*4*) proposed a theoretical model of the molecule but did not give any experimental structural information.

In the current study, we have synthesized cyclic RTD-1 as well as the open chain analogue oRTD-1 and elucidated their three-dimensional structures in solution with the aim of understanding their mode of action.

MATERIALS AND METHODS

Peptide Synthesis. (a) Chain Assembly. BOC-amino acids used in the chain assembly were purchased from Nova Biochem (San Diego, CA) and Neosystem (Strasbourg, France). BOC-Arg-phenylacetamidomethyl-resin (BOC-Arg-Pam-resin) was purchased from Applied Biosystems (Foster City, CA). The following side chain protecting groups were used: Arg(Tos), Cys(4-MeBzl), and Thr(Bzl). Chain assembly was performed on 0.5 mmol of BOC-Arg-Pam-resin, and the amino acids were coupled using activation with HBTU and DIEA. After each coupling step, a resin sample was taken and the acetylation efficiency was determined by quantitative Ninhydrin reaction (*13*). After completion of the chain assembly, the N-terminal BOC group was removed with TFA, and the resin was washed with DMF and dichloromethane and dried under a nitrogen atmosphere. Approximately 300 mg of dry resin was treated with 10 mL of HF/*p*-cresol/*p*-thiocresol (20:1:1 = vol/vol/vol) at 0 °C for 2 h. The residual HF was evaporated, the crude peptide was washed with cold diethyl ether, dissolved in 50% acetonitrile/water, and lyophilized. The crude lyophilized peptide was redissolved in 0.05% TFA/water, analyzed by analytical HPLC[1] and MS, finally purified on a preparative HPLC column, and lyophilized again.

(b) Oxidation. The crude peptide was dissolved in 1% acetic acid. After the pH was adjusted to 7.5 with ammonium hydroxide, the reaction mixture was stirred overnight at room temperature in an open flask. The state of the oxidation was checked by MS and analytical HPLC, and the oxidized peptide was purified using the column and conditions described below.

(c) Cyclization. Three different methods were tested for cyclization of the oxidized peptide. These involved the use of the following reagents: (i) HBTU and DIEA in DMF, (ii) BOP (Castro's reagent) and DIEA in DMF, and (iii) HOBt and EDC in DMSO (*4*). The cyclizations were monitored by HPLC and MS. The final purification was again done by preparative HPLC as described below.

(d) HPLC. Analytical reversed-phase HPLC was performed on an RP C18 column (Vydac C18, 5μm, 4.6 × 250 mm) using a 1%/min linear gradient of buffer B (90% acetonitrile, 10% water, 0.025% TFA) in buffer A (0.05% TFA in water) at a flow rate of 1 mL/min. For detection, an absorbance detector set to 214 nm was used. All the peptides were purified on a preparative HPLC column (Vydac C18, 10 μm, 2.2 × 25 cm) run at 8 mL/min using the same gradient and the same solvents as for the analytical runs.

NMR Spectroscopy. Samples for NMR spectroscopy contained 1 mM cyclic RTD-1 or its open chain analogue

[1] Abbreviations: HPLC: high performance liquid chromatography; MS: mass spectrometry; DMF: *N*,*N*-dimethylformamide; DMSO: dimethyl sulfoxide; DPC: dodecylphosphocholin; TFA: tetrafluoroacetic acid; HBTU: *O*-(benzotriazol-1-yl)-*N*,*N*,*N*′,*N*′-tetramethyluronium hexafluorophosphate; HOBt: 1-hydroxybenzotriazole; DIEA: diisopropyl-ethylamine; EDC: ethylenediaminecarbodiimide; BOP: benzotriazole-1-yl-oxy-tris-(dimethylamino)-phosphonium hexafluorophophate; 1D: one-dimensional; 2D: two-dimensional; NOE: nuclear Overhauser effect; NOESY: 2D NOE spectroscopy; TOCSY: total correlation spectroscopy; DQF-COSY: double quantum filtered 2D correlation spectroscopy; 3QF-COSY: triple quantum filtered 2D correlation spectroscopy; RMSD: root-mean-square deviation; ROESY: rotating frame Overhauser effect spectroscopy; ω: Larmor resonance frequency; τ_c: rotational correlation time of a molecule; the standard one letter and three letter codes are used for amino acids.

oRTD-1 and 20 mM sodium phosphate buffer in either 80% H_2O/10% D_2O/10% acetonitrile-d_3 (referred to as 10% acetonitrile in the following text) or 99% D_2O (referred to as 100% D_2O) at pH 4.5. For RTD-1, data from samples in 90% H_2O/10% D_2O (referred to as 100% water) at pH 4.5 and pH 3.5 served for confirmation of the assignments. The pH values are meter readings at 295 K, uncorrected for deuterium isotope effects.

(a) Data Acquisition. Spectra were recorded at 280, 300, or 310 K on Bruker ARX500 and DMX750 spectrometers with triple-resonance self-shielded z-gradient 5 mm probes. Quadrature detection in the indirect dimension was achieved using the TPPI (*14*) or the States-TPPI method (*15*). The spectral width was 10 ppm for both peptides, and the carrier was positioned on the water resonance. Water suppression in the COSY experiments was achieved using selective low-power irradiation of the water resonance during the relaxation delay of 1.3 s. For NOESY, ROESY, and TOCSY experiments a 3-9-19 WATERGATE (*16*) scheme was used, employing gradient pulses of $\sim$6Gcm^{-1} either side of a 10 kHz 3-9-19 binomial pulse. TOCSY experiments used the MLEV17 sequence (*17*) for isotropic mixing. Essentially the same pulse sequences were used for measurements in D_2O, except that no water suppression was necessary.

The following spectra were recorded on cyclic RTD-1 and linear oRTD-1: NOESY spectra (*18*) with 4096* $\times$ 512 data points in f1 and f2, respectively (* denotes complex data points), and mixing times of 120, 200, and 400 ms, TOCSY spectra (*19*) with 4096* $\times$ 512 data points and a spin-lock period of 80 ms, DQF-COSY spectra (*20*) with 4096* $\times$ 512 data points. The same set of spectra was recorded for both samples in 100% D_2O. Additionally, a 3QF-COSY spectrum (*21*) with 4096* $\times$ 256 data points was recorded of RTD-1 in 100% D_2O. Furthermore, a ROESY spectrum (*22*) with 4096* $\times$ 128 data points and a clean TOCSY (*23*) spectrum were recorded for RTD-1 in 10% acetonitrile at 310 K. However, these two experiments did not provide any additional information.

Disappearance of the amide proton signals on dissolution in D_2O was measured in a series of 1D spectra recorded starting 10 min after dissolution. For measuring the temperature dependence of the HN shifts, TOCSY spectra were recorded at 278, 287, and 313 K. Additionally, data from 1D spectra recorded at 280 and 300 K were used where possible (residues F2, R9, V11, and R18).

(b) Data Processing. Spectra were processed on a SGI Octane R12000 workstation using either XWINNMR (Bruker) as described previously or CCNMR (*24*). Data were analyzed using the program GLXCC (*24*).

(c) Structure Calculations. Distance constraints for structure calculations were derived from cross-peaks in NOESY spectra recorded at 750 MHz and 310 K (solvent: 10% acetonitrile) with a mixing time of 200 ms. The cross-peaks were classified according to their intensities and grouped into five categories (corresponding to upper bound interproton distance restraints of 2.5, 3.0, 3.5, 4.0, and 5.5 Å, respectively). Appropriate pseudoatom corrections were applied to non-stereospecifically assigned protons. Initial structures were generated using X-PLOR 3.851 (*25*). Several rounds of structure calculation and assignment were performed to resolve ambiguities. Dihedral angle constraints were generated after stereospecific assignment of side chain protons or deduced from $^3J_{(HN-H\alpha)}$ coupling constants. These coupling constants were obtained from line shape analysis of the antiphase cross-signal splitting in a high digital resolution 2D DQF-COSY spectrum and from NOESY and TOCSY cross-peaks following the method of Wang et al. (*26*).

For RTD-1 χ_1 angles of C3 and C7 were constrained to $-60 \pm 30°$ according to the NOE patterns. ϕ angle constraints of $-120 \pm 60°$ were inferred from $^3J_{(HN-H\alpha)}$ couplings of R9, C12, R13, and T17, while the ψ angle of T17 was constrained to $150 \pm 40°$, again according to NOE patterns. For oRTD-1, the χ_1 angles of F2 and V11 were restrained to $180 \pm 30°$, those of C3, C7, C16, and T17 were restrained to $-60 \pm 30°$ and the χ_1 angle of R9 was restrained to $60 \pm 30°$, all according to NOE patterns. Finally, constraints of $-120 \pm 30°$ on the ϕ angles of C3, V11, and I15 were inferred from $^3J_{(HN-H\alpha)}$ coupling constants.

The final sets of 100 structures for both peptides were calculated in CNS (*27*) using the standard dynamical annealing protocol and extended structures with correct local geometry as a starting point. The resulting structures were further refined by energy minimization in water, again using the standard protocol.

Finally, for each peptide 20 models with the lowest overall energies that had no violations of distance restraints > 0.3 Å or dihedral angle restraints $> 4.0°$ were retained for analysis. Structures were visualized using the programs InsightII (Biosym) and MOLMOL (*28*) and analyzed with PROMOTIF (*29*) and PROCHECK_NMR (*30*).

RESULTS

Synthesis. Assembly of the linear peptide chain proved to be straightforward. Although a few amino acids had to be double coupled, the average yield of the coupling reactions was 99.4%. HPLC and MS analyses confirmed the major product to be reduced, open chain RTD-1. Oxidation of this crude peptide yielded one major product. This was confirmed by MS to be the oxidized, open chain analogue oRTD-1, which was used in NMR experiments after purification.

The open chain analogue, oRTD-1, was cyclized via the formation of an amide bond between the carboxyl group of R18 and the amino group of G1. Generally, in cyclization reactions long reaction times increase the probability of side reactions and consequently the loss of product. Therefore we sought a fast, reliable method that also allowed for easy purification of the product. To establish the best reaction conditions for this cyclization, three methods were tested in small-scale experiments.

Method (i), involving the use of HBTU and DIEA in DMF, proved to be not feasible. HPLC analysis of the reaction mixture showed numerous peaks without a major product, indicating the presence of various side reactions.

Method (ii) turned out to be the fastest. Using BOP (Castro's reagent) and DIEA in DMF all the starting material had reacted within less than 12 h. The HPLC trace of the reaction mixture showed one major product. Unfortunately, this major product, cyclic oxidized RTD-1 as confirmed by MS, almost coeluted with excess reagents, making the purification difficult.

With method (iii), using HOBt and EDC in DMSO, the reaction took about 20 h to complete. The HPLC trace

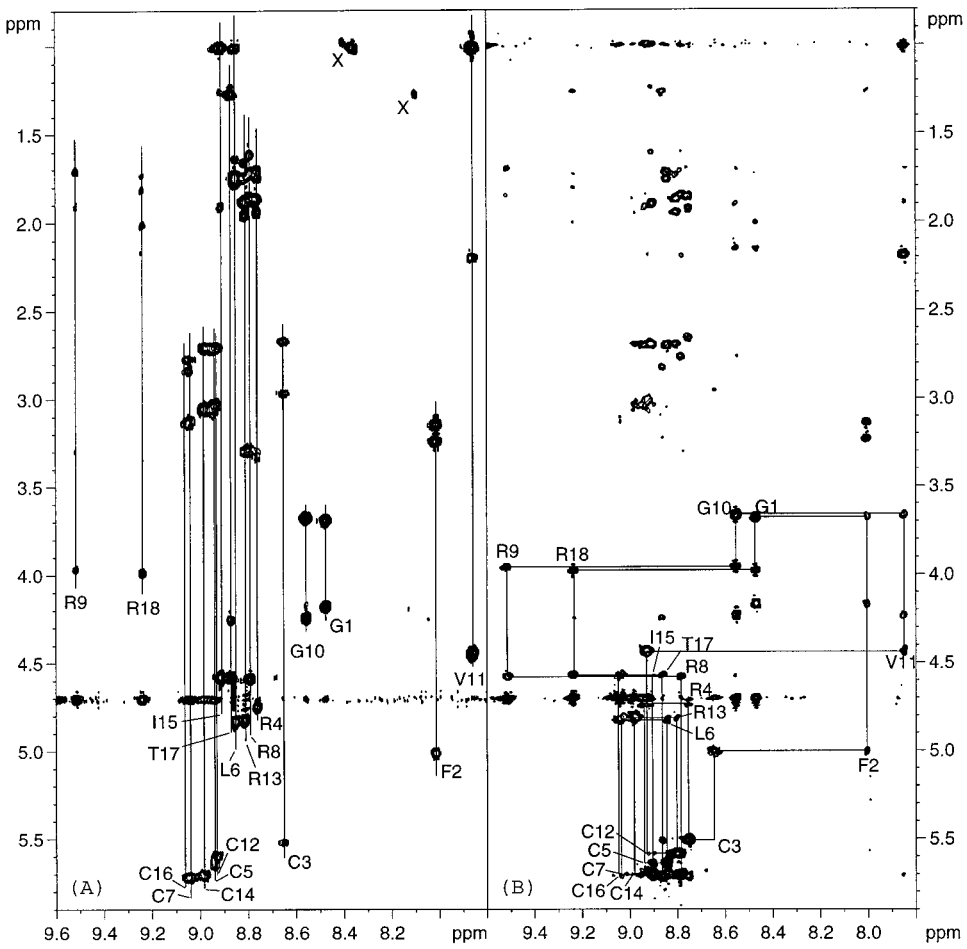

FIGURE 2: Fingerprint region of the TOCSY (A) and NOESY (B) spectra of RTD-1 in 10% acetonitrile-d_3 (pH 4.5) collected at 310 K at 750 MHz. The sequential connectivity pattern shown confirms the cyclic nature of the peptide backbone. The peaks labeled with X in the TOCSY are artifacts of an antidiagonal.

showed one major product, which was readily purified and identified by MS as cyclic, oxidized RTD-1.

Although workup was more difficult for method (ii), both methods (ii) and (iii) were used for bulk cyclizations.

In the initial characterization, the disulfide pattern of RTD-1 was determined by mass spectral analysis of protease digestion fragments produced by sequential digestion with trypsin and thermolysin (*4*). In the current study, oxidation of the reduced peptide using the same procedure as Tang et al. (*4*) gave rise to a single product which, after cyclization, showed the same HPLC elution profile as native RTD-1. The presence of NOEs (mentioned later) between Hα proton pairs of all three disulfide bridges as well as a statistical analysis of inter-sulfur distances in trial calculations without disulfide bond constraints (also mentioned later) confirmed the correct cystine connectivities.

NMR Spectroscopy. Both peptides were soluble in water as well as in 10% acetonitrile. The solutions remained stable for several weeks without showing any signs of aggregation or precipitation. In aqueous solution, the resonances in the amide region of the TOCSY spectra were partially overlapped, which made the assignment difficult. This problem was overcome by varying the solvent system and the temperature at which the spectra were acquired. The spin systems of the individual amino acids were identified and assigned to specific residues in the sequence using the data from NOESY experiments. Figure 2 shows regions of the 750 MHz NOESY and TOCSY spectra of RTD-1 with sequential assignments indicated. As can clearly be seen, the cycle of Hα-HN sequential connectivities is unbroken, confirming the cyclic nature of RTD-1.

The corresponding data for oRTD-1 are generally quite similar except for residues G1 and R18. The similarity of the spectra indicates that both peptides have rather similar conformations in solution.

For both peptides, the NOESY cross-peaks were of negative sign, i.e., in phase with the diagonal peaks, suggesting that the correlation time of the peptides is within the slow tumbling regime ($\omega\tau_c > 1$). ROESY experiments did not provide any improvement of the data.

Secondary chemical shifts (Figure 3) (*31*) for the backbone Hα protons of both cyclic RTD-1 and oRTD-1 were calculated using the measured chemical shifts and the random coil values given in (*32*). For cyclic RTD-1, most of the Hα protons have chemical shifts that differ from the random coil values by more than 0.1 ppm, with many approaching 1 ppm, suggesting a highly structured molecule. Extended conformations are usually indicated by three or more successive secondary chemical shifts with clearly positive values. Thus, the secondary chemical shifts of residues F2 to R8 and V11 to T17 give a first hint toward an extended structure in these regions. The secondary chemical shifts for oRTD-1, also shown in Figure 3, again indicate a high similarity between

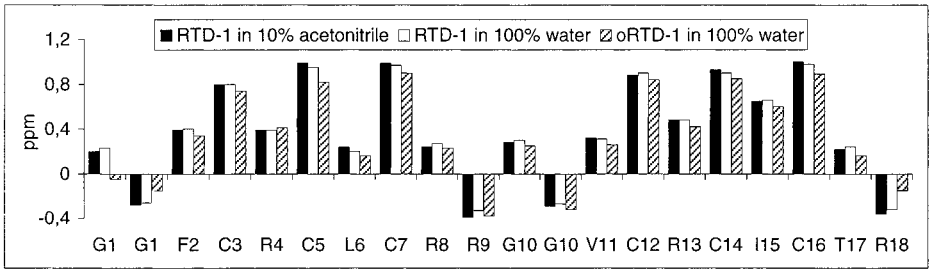

FIGURE 3: Comparison of the secondary chemical shifts of the Hα protons. Black: RTD-1 in 10% acetonitrile; white: RTD-1 in 100% water; shaded: oRTD-1 in 100% water, all at 310 K and pH 4.5. The similarity in secondary chemical shifts indicates that the three-dimensional structures of all three peptides are rather similar.

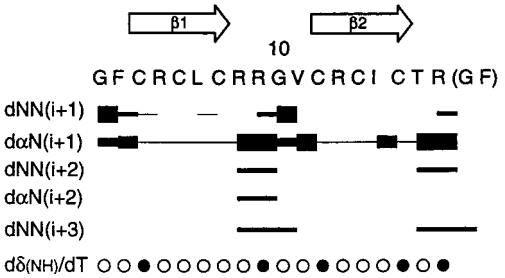

FIGURE 4: Summary of the sequential and medium-range NOE connectivities for RTD-1. The thickness of the filled bars corresponds to the NOE intensities. Thin lines indicate residues where the NOE intensities could not reliably be determined because of overlap. Backbone amide protons with temperature coefficients < 5 ppb/K, that are shielded from interaction with the solvent, are indicated by filled circles. The position of the two β-strands, deduced from chemical shifts and NOE data, is shown above the sequence. Two residues (GF) are bracketed to emphasize the cyclic nature of the peptide sequence.

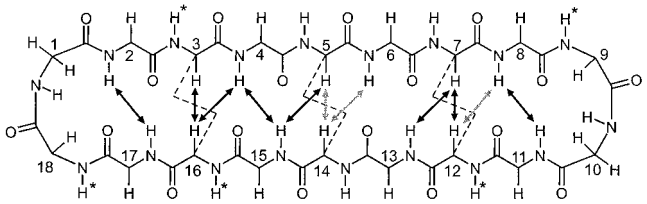

FIGURE 5: Schematic diagram of the backbone interstrand NOEs in RTD-1, comprising medium- and long-range NH-NH, NH-Hα, and Hα-Hα NOEs. The gray arrows correspond to NOEs that are ambiguous due to overlap. The three disulfide bonds are indicated by broken lines. Amide protons with a low temperature coefficient are indicated by an asterisk. The α-carbons are labeled with the number of the corresponding residue. For clarity, all sequential NOEs as well as some medium-range NOEs in the two turn regions are not shown. (NOESY data measured in 100% water at pH 4.5, 310 K, and 750 MHz)

the solution structures of RTD-1 and its open chain analogue oRTD-1.

Secondary shifts of the Hα protons (Figure 3) also served to confirm that RTD-1 adopts the same conformation in 10% acetonitrile-d_3 as it does in water. For RTD-1, the average change in secondary shifts on addition of 10% acetonitrile-d_3 was 0.02 ppm for all 20 Hα protons. This result and the obvious similarity of the spectra measured in both solvent systems confirmed that RTD-1 adopts the same three-dimensional fold in both solvent systems.

The pattern of sequential and medium-range NOE connectivities for RTD-1 is shown in Figure 4. These data as well as the observed long-range backbone NOEs (Figure 5) clearly support the chemical shift data, suggesting that the region between residues F2 and R8 and V11 and T17 is actually a well-defined antiparallel β-sheet.

Figures 4 and 5 also show the HN protons of RTD-1 that have low temperature coefficients. Low temperature coefficients can be an indicator of hydrogen bonding (*33*), but this is not always the case, especially in small, flexible peptides (*34*). Five amide protons with temperature coefficients < 5 ppb/K were identified and assigned to residues C3, R9, C12, C16, and R18. On dissolution of the lyophilized peptide in D_2O, all the amide signals disappeared within 10 min. Since D_2O exchange data are a more reliable indicator of hydrogen bonding than temperature coefficients and no NH signals were found to be slow exchanging, no hydrogen bond constraints were included in the structure calculations.

Structure Calculations. For cyclic RTD-1, a total of 82 distance constraints comprising 57 sequential and 25 medium- and long-range NOEs (list provided in Supporting Information) was used in structure calculations. No intraresidual distance constraints or hydrogen bonds were included in the calculations. Dihedral angle constraints were generated after stereospecific assignment of side chain protons or deduced from $^3J_{(HN-H\alpha)}$ coupling constants. Constraints for four ϕ angles, one ψ angle, and two χ_1 angles were inferred from these data.

To confirm the disulfide bond pattern, preliminary structure calculations were done in the absence of defined disulfide bonds. The individual distances between all the possible pairs of sulfur atoms were then compared with ideal S−S bonding distances. In a statistical analysis of the 15 possible sets of disulfide bonds, the previously demonstrated (*4*) connectivity pattern (3−16, 5−14, and 7−12) clearly showed the lowest RMSD, confirming that this pattern is the most consistent with the NMR data (see also supplementary data). This disulfide bonding pattern was incorporated into the final round of structure calculations.

Of the 100 structures calculated, 20 were selected on the basis of low overall energy and low violations to represent the solution structure of RTD-1. Figure 6 shows a ribbon representation of one of the lowest energy structures and a superposition of the turn regions (T17 to F2 and R8 to V11) of these 20 structures. The average pairwise backbone RMSD for the two turns is 0.07 Å over residues T17 to F2 and 0.08 Å over residues R8 to V11, respectively. Despite the excellent superposition over the turn regions (see Figure 6, panel B), the superposition over the whole molecule is poor (RMSD 1.55 Å over all backbone atoms and 1.03 Å over the β-sheet, respectively). It appears that the molecule adopts a closed β-hairpin structure but that there is variability in the central region, so that the orientation of the two turns with respect to one another is not well defined. This is

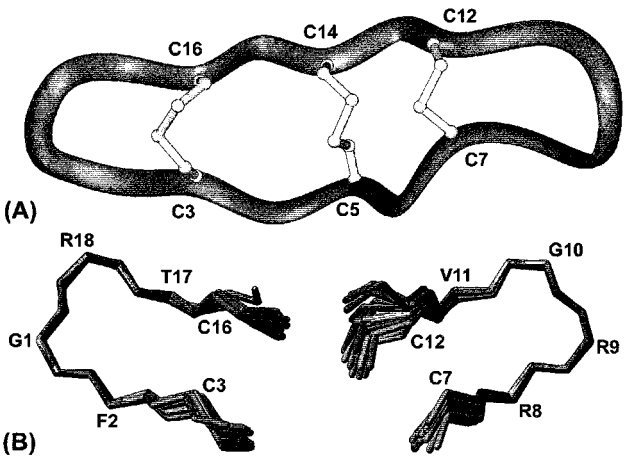

FIGURE 6: (A) Ribbon diagram of one of the lowest energy structures of RTD-1. The disulfide bonds are shown as balls and sticks. (B) The turn regions of RTD-1 (residues C16−C3, left; residues C7−C12, right) superimposed over the backbone atoms of T17−F2 and R8−V11, respectively. For clarity, the α-carbon atoms of selected residues are labeled in both figures. While the loops are very well defined within themselves, the β-sheet fragments shown (residues C3, C16, C7, and C12) clearly indicate the flexibility of the loops with respect to the rest of the molecule.

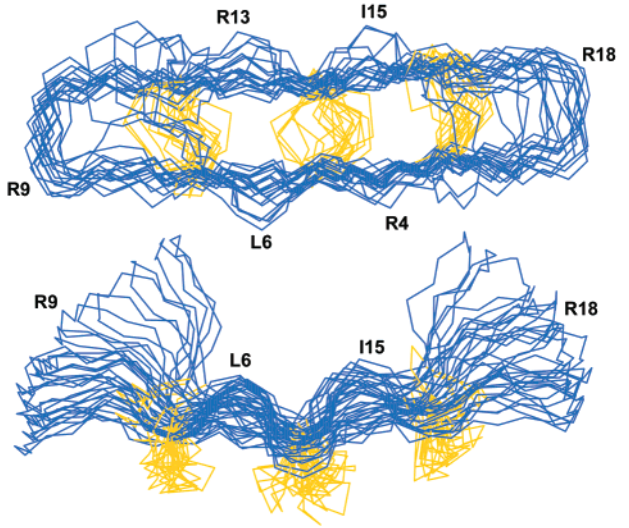

FIGURE 7: Superposition of 20 of the lowest energy structures of RTD-1 over the backbone atoms of the β-sheet region (residues C3−C7 and C12−C16), with the disulfide bridges given in yellow. The figure clearly shows the flexibility of the two turns with respect to the β-sheet region.

consistent with the fact that no slowly exchanging amide signals, that would normally be associated with a well-defined β-sheet, were observed. While it is most likely that the variability of RTD-1 observed in the structure calculations reflects an inherent flexibility of the molecule, relaxation experiments would be needed to confirm this. Figure 7 shows a superposition of the 20 structures which illustrates the lack of a tightly defined relative orientation of the turn and β-strand regions.

Geometric and energetic statistics for the 20 selected structures of RTD-1 are given in Table 1. Because of the flexibility of RTD-1, these statistics tend to underestimate the quality of the structure calculations in the ordered regions and thus should be interpreted with caution. However, it is also important to stress that the presence of flexibility means that the derived structures should be interpreted only in a qualitative way, with due regard for the limitations inherent in data from flexible peptides.

Table 1: Parameters Characterizing the Structure Families of RTD-1 and oRTD-1 in Solution[a]

parameter	⟨RTD-1⟩	⟨oRTD-1⟩
Deviations from Idealized Geometry		
bond lengths (Å) (286/288)	0.003 ± 0.000	0.004 ± 0.000
angles (deg) (511/518)	0.463 ± 0.031	0.547 ± 0.058
impropers (deg) (84/83)	0.296 ± 0.030	0.309 ± 0.051
Energies (kcal mol^{-1})		
E_{NOE}	8.41 ± 2.14	9.41 ± 4.28
E_{tor}	0.09 ± 0.16	0.67 ± 0.61
E_{vdW}	−42.70 ± 8.37	−22.06 ± 9.69
E_{bond}	3.15 ± 0.36	4.20 ± 0.90
E_{angle}	16.76 ± 2.27	23.66 ± 5.08
E_{impr}	2.08 ± 0.43	2.29 ± 0.74
E_{total}	−490.27 ± 25.09	−575.31 ± 43.17
Number of Residual Constraint Violations for all Distance Constraints		
RMSD ≥ 0.2 Å	0.85 ± 0.85	1.10 ± 1.14
maximum violation (Å)	0.274	0.292
RMSD from Experimental Constraints		
distance constraints (Å) (82/55)	0.046 ± 0.006	0.058 ± 0.013
dihedral constraints (deg) (7/10)	0.322 ± 0.330	0.978 ± 0.384
Ramachandran Statistics (Except Gly and Pro Residues):		
residues in most favored regions	56.7%	30.7%
residues in additionally allowed regions	39.7%	63.0%
residues in generously allowed regions	1.7%	5.3%
residues in disallowed regions	2.0%	1.0%

[a] ⟨RTD-1⟩ and ⟨oRTD-1⟩ represent the ensembles of the 20 final structures of cyclic RTD-1 and its open chain analogue oRTD-1, respectively. The number of bonds, angles, impropers, and constraints for both molecules is given in parentheses (in the order RTD-1/oRTD-1).

For oRTD-1, 43 sequential and 11 medium- and long-range distance constraints were used for structure calculations. Again, no intra-residual distance constraints or hydrogen bonds were included. Dihedral constraints were inferred for three ϕ angles and seven χ_1 angles. Of the 100 structures calculated, again 20 structures were selected on the basis of low overall energy and low violations to represent the solution structure of oRTD-1. The turn region (R8 to V11) of these 20 structures superimposed over the backbone atoms is shown in Figure 8 together with the respective region of RTD-1. The average pairwise backbone RMSD for the turn in the 20 oRTD-1 structures is 0.38 Å.

DISCUSSION

Three-Dimensional Structures of RTD-1 and oRTD-1. In the current study, we have determined the three-dimensional structures of RTD-1, a cyclic antimicrobial peptide originally isolated from rhesus macaque leukocytes (*4*), and its open chain analogue, oRTD-1. Despite the constraints introduced by its cyclic backbone and triple disulfide linkage, RTD-1 appears to exhibit a considerable degree of flexibility in solution. While several NMR markers, including the very significant downfield Hα shifts of residues F2 to R8 and V11 to T17 and a series of interstrand NOE connectivities, clearly indicate the presence of a β-sheet type structure, the

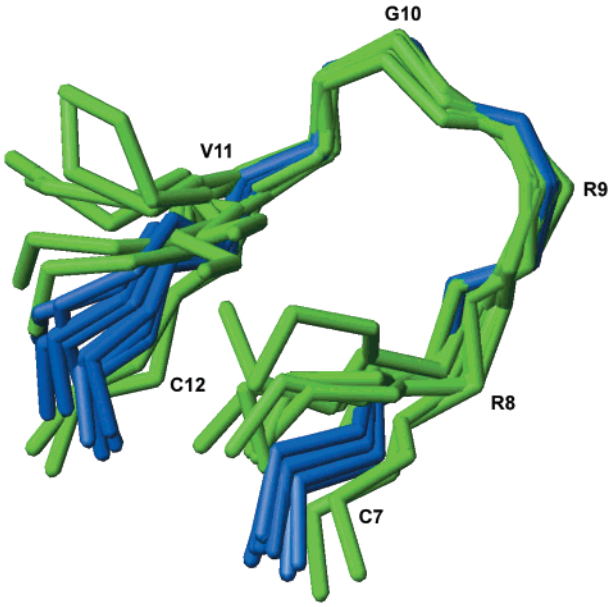

FIGURE 8: Superposition of the turn region (C7−C12) of 10 of the lowest energy structures of oRTD-1 (in green) with the corresponding residues of 10 structures of RTD-1 (in blue), over the backbone atoms of R8−V11. The α-carbon atoms of selected residues are labeled. It can clearly be seen that the break in the peptide backbone between residues R18 and G1 does not change the loop conformation in oRTD-1.

calculated family of structures superimpose rather poorly, indicating the lack of a single, defined conformation. This is most likely due to bending motions at the center of the peptide.

In contrast to the flexible center of the peptide, the two turns at either end of the molecule are very well defined within themselves. The flexible core means that their relative orientation with respect to the β-sheet or with respect to each other is not defined. Both turns contain a glycine at position (i+2), which is typical for type II β-hairpins. However, the NOE patterns as well as the dihedral angles measured in the final family of 20 structures show the turns to be of type IV. For the lowest energy structure of RTD-1 the dihedral angles ϕ_2/ψ_2 and ϕ_3/ψ_3 are −63°/87° and 145°/−28° for the turn T17-F2 and −61°/78° and 136°/−23° for the turn R8−V11, respectively.

The very similar spectra of RTD-1 and its open chain analogue, oRTD-1, determined experimentally in the current study suggest that both peptides adopt analogous structures in solution. Indeed, the family of structure models of oRTD-1 exhibits a similar overall fold as cyclic RTD-1, albeit with a lower precision due to the lower number of constraints. The superposition of the turn region R8−V11 of the two peptides, given in Figure 8, shows that the turn is in principle not influenced by the breaking of the peptide backbone at the other end of the molecule.

While multiple disulfide bonds between two β-strands that are far apart in the sequence but close in space are fairly common in proteins, there are few naturally occurring peptides or proteins with a cystine bridge connecting two directly adjacent antiparallel strands of a β-sheet. Examples include SFTI-1, a trypsin inhibitor from sunflower seeds (*35*), and leucocin A, a type IIa bacteriocin from lactic acid bacteria (*36*). In some antimicrobial peptides, like protegrin-1 (PG-1), isolated from porcine leucocytes (*37*, *38*), or the

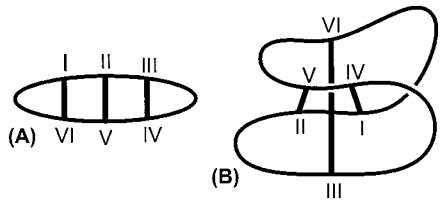

FIGURE 9: Schematic representation of laddered and braced disulfide arrangements exemplified by (A) RTD-1 and (B) the cyclotides.

tachyplesins (*39*), the two adjacent β-strands are connected by two disulfide bonds, but to our knowledge, RTD-1 is the only natural peptide discovered so far with three disulfide bonds linking the same two adjacent strands of a β-sheet. The unproblematic synthesis and folding of both RTD-1 and structurally analogous peptide templates based on the sequences of PG-1 (*40*) and tachyplesin-1 (*41*) indicates that this highly cross-linked structure is energetically favorable.

Comparison of RTD-1 with Other Cyclic, Disulfide-Bonded Peptides. NOEs between the Hα protons of C3 and C16, C5 and C14, and C7 and C12, respectively, confirm the unusual disulfide linkage pattern of RTD-1. This ladder-like arrangement of the three disulfide bonds, described by the connectivity pattern I−VI, II−V, and III−IV, distinguishes RTD-1 from other defensins as well as other polypeptides containing three disulfide bonds. For defensins, one criterion to differentiate between the α- and β-subgroups as well as insect defensins is the connectivity of the conserved cysteines. While β-defensins show a I−V, II−IV, III−VI pattern, α-defensins are characterized by a I−VI, II−IV, III−V pattern. Insect defensins show a different pattern again, summarized by the connectivities I−IV, II−V, and III−VI (*6*, *11*). A further motif, called the cystine knot, displays the same connectivity pattern as insect defensins. However, in that case two of the disulfide bonds form an embedded loop completed by the backbone fragments connecting the cysteine residues, while the third disulfide bond threads through this loop to form the cystine knot. Various small peptides, like the plant cyclotides (*12*), certain animal toxins (*42*), as well as larger biologically active proteins, for example, growth factors (*43*), are known to incorporate this motif.

Besides RTD-1, the plant cyclotides (*12*) are the only other naturally occurring family of cyclic tri-disulfide peptides. The cyclotides display weak antimicrobial and antifungal activity, but have quite a different structure from RTD-1. They typically contain about 30 amino acids arranged in a cyclic backbone, which is braced by three cross-linking disulfide bonds that form the cystine knot motif. In contrast to RTD-1, the structures of the cyclotides are exceptionally well defined (*12*, *44*, *45*), consisting of a distorted triple-stranded β-sheet, several β-turns, and the cystine knot core (*42*). The knotted arrangement of the disulfide-bonded core renders the backbone quite rigid and allows a precisely defined presentation of surface-active amino acid residues. The contrast in stability with RTD-1 is illustrated by the fact that up to one-third of all amide protons in the cyclotides are slowly exchanging in D_2O solution (*44*, *45*), whereas none of the amide protons in RTD-1 are slowly exchanging. The smaller size of RTD-1 and hence its higher cysteine content (6/18 vs 6/30 residues) might lead to the expectation that RTD-1 would be less flexible owing to a higher relative degree of cross-linking disulfide bonds. However, the op-

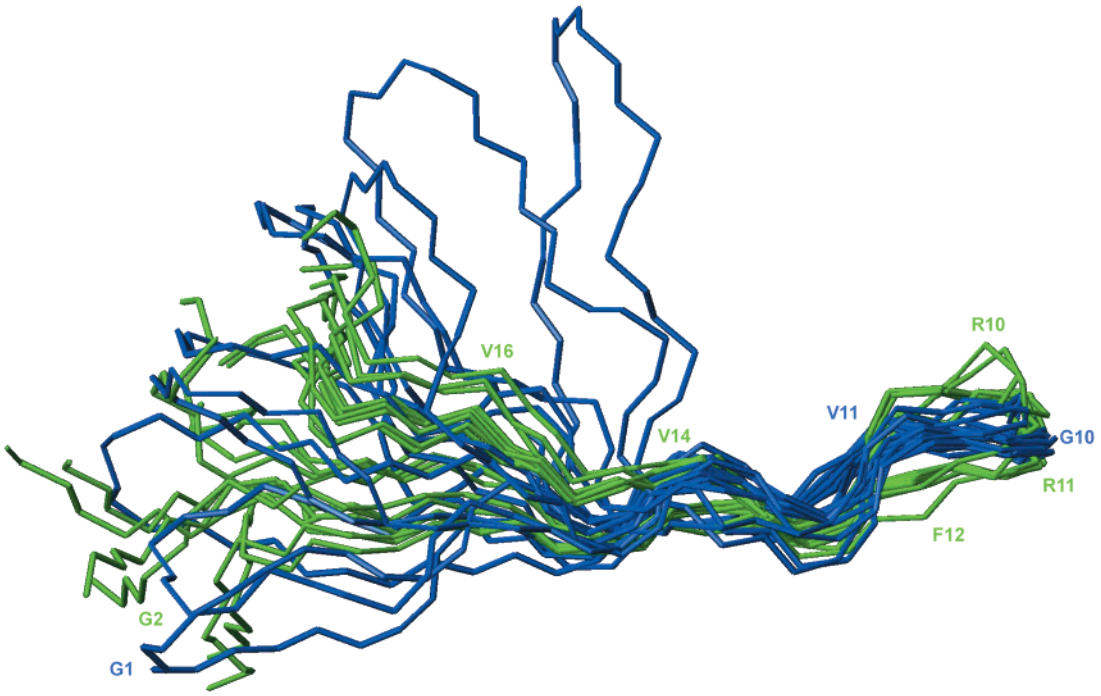

FIGURE 10: Superposition of 10 of the lowest energy structures of RTD-1 (blue) with 10 structures of PG-1 (green, PDB access code 1PG1). The structures are superimposed over the backbone atoms of the turn and the β-sheet of PG-1 (residues C6−C15 for PG-1 and residues C5−C14 for RTD-1, respectively), with selected α-carbons labeled in the colors of the corresponding peptide. While a certain degree of similarity can be seen, the superposition clearly shows the higher variability of RTD-1 as compared to PG-1.

posite is the case. Indeed, from an engineering perspective the laddered cross-linking in RTD-1 can be regarded as a wasteful use of disulfide bonds relative to the diagonal braced and interlocked arrangement in the cyclotides (Figure 9).

The surprising degree of flexibility of RTD-1 is further emphasized by a comparison of RTD-1 with SFTI-1 (*35*), a cyclic peptide of 14 amino acids that also adopts a structure of an antiparallel β-sheet linked by two β-turns. In contrast to RTD-1, the two strands of the β-sheet in SFTI-1 are connected only by one disulfide bond. Although SFTI-1 is significantly less cross-linked than RTD-1, it exhibits a marked degree of stability in complex with trypsin (*35*). Recent studies suggest that even in solution SFTI-1 is exceptionally well defined (D. Craik, M. Korsinczky, unpublished results). In light of these comparisons, it seems even more surprising that RTD-1 with its high degree of cross-linkage exhibits such a high flexibility. The fact that a single disulfide bond leads to effective stabilization of SFTI-1, but three disulfide bonds are less effective in RTD-1, again suggests a degree of waste in the disulfide bond engineering of RTD-1. Alternatively, the sequence of RTD-1 may be less amenable to cross-strand stabilization.

Structural Comparison of RTD-1 and Protegrin-1. Another molecule displaying the same unusual, ladder-like structure of cysteine connectivities as RTD-1 is PG-1. However, in contrast to RTD-1 PG-1 is not head-to-tail cyclized, only contains four cysteines, and therefore the two strands of its β-sheet are only stabilized by two rungs of disulfide bonds (*37*, *38*). PG-1 forms a relatively well-defined structure in solution, composed of a double stranded antiparallel β-sheet, with the strands connected by a β-turn and stabilized by the two disulfide bonds (*37*, *38*). Figure 10 shows the superposition of 10 of the lowest energy structures of RTD-1 with 10 structures of PG-1.

In both PG-1 and RTD-1, the turns are flexible with respect to the β-sheet part of the molecule, resembling the motion of a hinge (*37*, *38*). In RTD-1, the flexibility is confirmed by the fast exchange of all the amide protons potentially involved in hydrogen bonds in the β-sheet, as well as the high temperature coefficients of their chemical shifts. A similar result applies for PG-1. Although the β-sheet of PG-1 is relatively well defined in aqueous solution, all the potential cross-sheet amide protons exchange within 5 min. However, in the presence of dodecylphosphocholine (DCP), a detergent used to solubilize membrane peptides, all these protons were found to be slow exchanging, indicating better structuring of PG-1 in micelles (*46*). It will be interesting to see if similar stabilization occurs for RTD-1.

Structure−Activity Relationships in Cyclic and Linear Variants of RTD-1, PG-1, and Tachyplesin-1. Results of studies with truncated forms and disulfide variants of PG-1 suggest that residues 5−16, making up the β-sheet and the turn of PG-1, including three consecutive arginine residues, are principally responsible for its activity against *Neisseria gonorrheae* (*47*). The corresponding parts of RTD-1 contain residues R4−I15, including two consecutive arginines R8 and R9 in the turn region. Tam et al. (*40*) synthesized six cyclic analogues of PG-1 with zero to three disulfide bonds. One of these analogues, ccPG, closely resembles RTD-1 in its overall appearance, containing 18 amino acids and three evenly spaced disulfide bonds. However, while in RTD-1 the arginine residues are more or less evenly distributed within the molecule, the five arginines of ccPG are clustered in its two turns, resulting in two positively charged turn regions and a hydrophobic patch in the middle. The antimicrobial activity of this ccPG was similar to or weaker than that of PG-1 against 10 tested organisms (Gram-positive and Gram-negative bacteria as well as fungi), but its

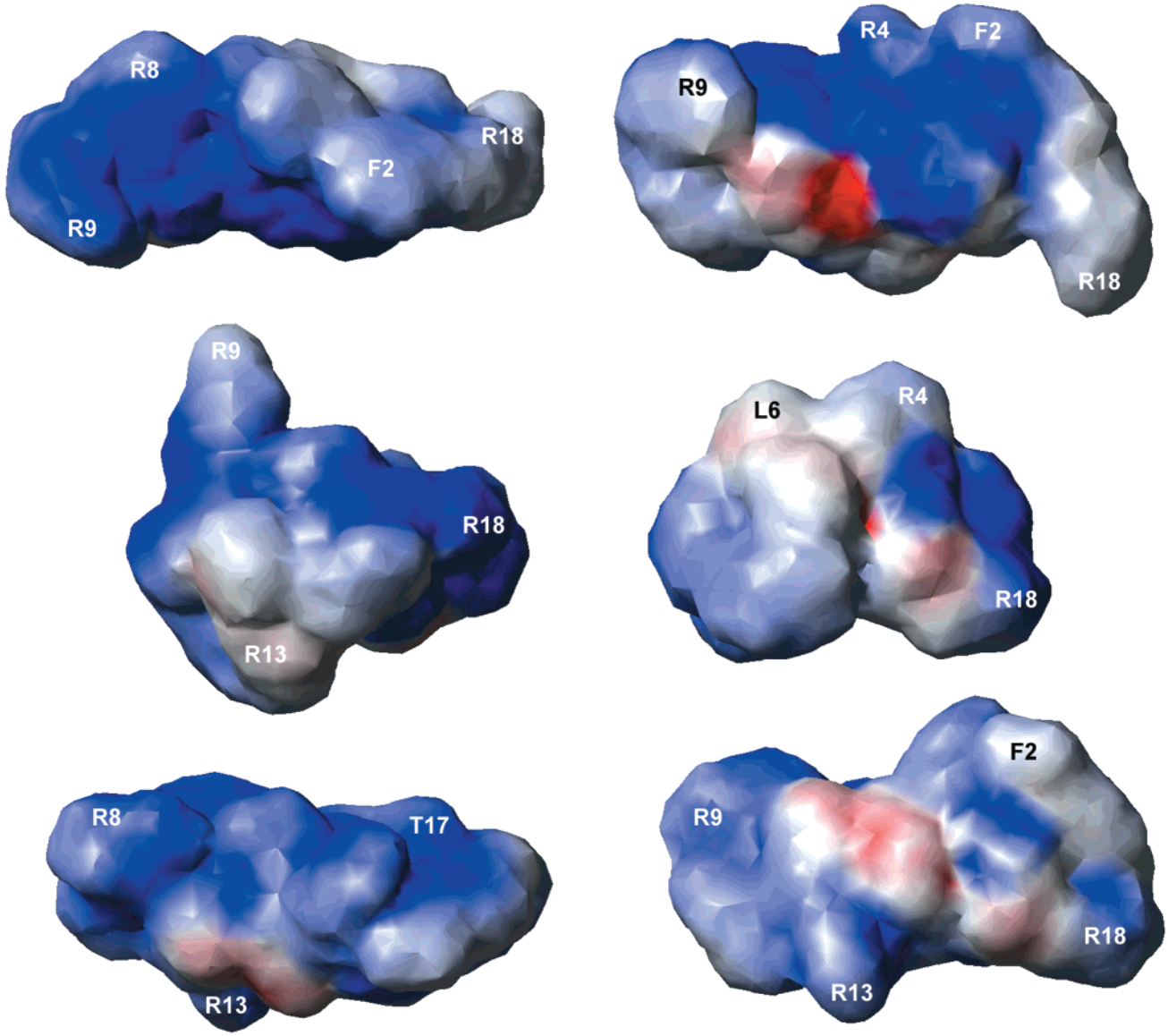

FIGURE 11: Electrostatic potential surface of three representative structures of RTD-1. Positively charged areas are colored in blue, negatively charged areas are in red and uncharged ones are in white. Although the positively charged areas are clustered in all models, there is no clear separation between charged and hydrophobic regions such as in other antimicrobial peptides.

hemolytic activity against human erythrocytes was about 10 times less than that of PG-1. Tam et al. (*40*) linked the significantly lower cytotoxicity of the cyclic three-disulfide analogue of PG-1 to the assumption that it would have a highly constrained, rigid nature. No structural studies were undertaken, and while it is likely that the cyclic derivatives are more rigid than acyclic ones, our experimental data show that at least RTD-1 is not completely rigid. Tam et al. (*41*) also synthesized six cyclic analogues of tachyplesin-1, including two resembling RTD-1 in both overall appearance and distribution of the arginines. Again, they associated the lower antimicrobial activity against 10 tested microorganisms and the marked decrease in cytotoxicity with the assumed rigid structure of the cyclic analogues.

According to Tang et al. (*4*) oRTD-1 is three times less active against *Staphylococcus aureus* and *Escherichia coli* than cyclic RTD-1. The authors (*4*) attributed this loss of activity to the two additional charges at the termini of acyclic oRTD-1 rather than to a change in the overall structure or mobility of the peptide. The two additional charges at the termini of acyclic oRTD-1 were proposed to render the molecule less efficient in binding to and consequently inserting into target cell membranes (*4*). Our findings that there are no significant conformational differences between the two peptides, as well as no differences in the overall flexibility support this theory by eliminating alternative explanations based on entropic (flexibility) differences or on specific conformational changes.

Mechanism of Activity of Antimicrobial Peptides. In a recent report Huang (*2*) suggested a two-stage process for the action of both helical and β-sheet antimicrobial peptides. At low peptide-to-lipid ratios (P/L), it was proposed that the peptides are adsorbed in the lipid headgroup region of the cell membrane in a functionally inactive state, whereas above a certain threshold value of P/L the peptides form pores in the cell membrane, which are lethal to the cell. The most important common characteristic of the peptides examined in that study (magainin 2, the magainin analogue MSI-78, PG-1, the protegrin analogue IB367, alamethicin I, and melittin) was their cylindrical shape: hydrophobic on one side of the cylindrical axis and hydrophilic on the other. The theoretical model for RTD-1 (*4*) shows the arginine side

chains sticking out like spikes, which is confirmed by the experimentally determined structures reported here, making it difficult to picture RTD-1 as an amphiphilic molecule. Figure 11 shows surface models of three representative structures of RTD-1. While all three models show a certain degree of clustering of the charged residues, none exhibits a clearly amphiphilic character. The structural studies reported here thus help to eliminate this type of mechanism for the antimicrobial activity of RTD-1.

Other mechanisms for the antimicrobial activity of β-sheet peptides have been proposed, including those that involve oligomer formation. Indeed, Roumestand et al. (*46*) noted that the structure of PG-1 becomes better defined in the presence of DCP micelles and reported intermolecular NOEs consistent with oligomer formation. In light of the current study, it seems likely that RTD-1, like PG-1, may adopt a more rigid three-dimensional fold upon interaction with a membrane lipid bilayer, rather than its flexibility being the cause of its antimicrobial action. However, to further investigate this theory NMR experiments with RTD-1 in the presence of model membranes or micelles have to be carried out. It is interesting that while no slow exchange amide signals were observed for RTD-1 in water, several amide protons on the periphery of the β-strand structure had low temperature coefficients consistent with weak hydrogen bonds in a dimeric or oligomeric structure. Such potential interactions could be markedly enhanced in the presence of a membrane, as reported for PG-1.

Summary. The data presented in this study shows that RTD-1 and its open chain analogue oRTD-1 adopt analogous three-dimensional structures. Considerable parts of both peptides, namely, the β-sheet regions between residues C3 and C7, and C12 and C16, respectively, lack a single, defined structure in solution. However, the turns are well defined within themselves and seem to be flexible with respect to the extended regions of the molecule. Although the two strands of the β-sheet are connected by three disulfide bonds, this region displays a degree of flexibility. Some amide protons that should be solvent-exposed in a monomeric β-sheet structure show low temperature coefficients, suggesting the possible presence of weak intermolecular hydrogen bonds. NMR experiments with RTD-1 and DPC micelles could confirm whether RTD-1 forms dimeric or oligomeric structures in the presence of membranes. Furthermore, to fully assess the flexibility of RTD-1 and its open chain analogue, oRTD-1, relaxation experiments would be necessary.

ACKNOWLEDGMENT

D.C. is an Australian Research Council Professorial Fellow. The Institute for Molecular Bioscience is a Special Research Centre of the Australian Research Council. M.T. thanks Graz University of Technology and the IMB for a scholarship. We thank Paul Alewood and Paramjit Bansal (IMB) for helpful advice on the synthesis of RTD-1. M.T. expresses her special thanks to Walter Steiner (Graz University of Technology) for his benevolence and support.

SUPPORTING INFORMATION AVAILABLE

All ^{1}H chemical shifts of both cyclic RTD-1 and the open chain analogue oRTD-1 are given in the Supporting Information. The Supporting Information furthermore includes details of the statistical analysis of S−S distances and a table with the medium- and long-range NOE restraints used in the structure calculations of RTD-1. This material is available free of charge via the Internet at http://pubs.acs.org.

REFERENCES

1. Lehrer, R. I., Lichtenstein, A. K., and Ganz, T. (1993) *Annu. Rev. Immunology 11*, 105−128.
2. Huang, H. W. (2000) *Biochemistry 39*, 8347−8352.
3. Heller, W. T., Waring, A. J., Lehrer, R. I., Harroun, T. A., Weiss, T. M., Yang, L., and Huang, H. W. (2000) *Biochemistry 39*, 139−145.
4. Tang, Y.-Q., Yuan, J., Ösapay, G., Ösapay, K., Tran, D., Miller, C. J., Oullette, A. J., and Selsted, M. E. (1999) *Science 286*, 498−502.
5. Martin, E., Ganz, T., and Lehrer, R. I. (1995) *J. Leukocyte Biol. 58*, 128−136.
6. White, S. H., Wimley, W. C., and Selsted, M. E. (1995) *Curr. Opinion Struct. Biol. 5*, 521−527.
7. Zeya, H. I., and Spitznagel, J. K. (1966) *J. Bacteriol. 91*, 750−754.
8. Ganz, T., Selsted, M. E., Szklarek, D., Harwig, S. S. L., Daher, K., Bainton, D. F., and Lehrer, R. I. (1985) *J. Clin. Invest. 76*, 1427−1435.
9. Miyanoshita, A., Hara, S., Sugiyama, M., Asaoka, A., Taniai, K., Yukuhiro, F., and Yamakawa, M. (1996) *Biochem. Biophys. Res. Commun. 220*, 526−531.
10. Broekaert, W. F., Terras, F. R., Cammue, B. P., and Osborn, R. W. (1995) *Plant Physiol. 108*, 1353−1358.
11. Diamond, G., and Bevins, C. L. (1998) *Clin. Immunol. Immunopathol. 88*, 221−225.
12. Craik, D. J., Daly, N. L., Bond T., and Waine C. (1999) *J. Mol. Biol. 294*, 1327−1336.
13. Sarin, V.K., Kent, S. B. H., Tam, J. P., and Merrifield, R. B. (1981) *Anal. Biochem. 117*, 147−157.
14. Marion, D., and Wüthrich, K. (1983) *Biochem. Biophys. Res. Commun. 113*, 967−974.
15. Marion, D., Ikura, M., Tschudin, R., and Bax, A. (1989) *J. Magn. Reson. 85*, 393−399.
16. Sklenar, V., Piotto, M., Leppik, R., and Saudek, V. (1993) *J. Magn. Reson. A 102*, 241−245.
17. Bax, A., and Davies, D. G. (1985) *J. Magn. Reson. 65*, 355−360.
18. Kumar, A., Ernst, R. R., and Wüthrich, K. (1980) *Biochem. Biophys. Res. Commun. 95*, 1−6.
19. Braunschweiler, L., and Ernst, R. R. (1983) *J. Magn. Reson. 65*, 521−528.
20. Rance, M., Sørensen, O. W., Wagner, G., Ernst, R. R. and Wüthrich, K. (1983) *Biochem. Biophys. Res. Commun. 117*, 479−485.
21. Shaka, A. J., and Freeman, R. (1983) *J. Magn. Res. 51*, 169−173.
22. Bothner-By, A. A., Stephens, R. L., Lee, J.-M., Warren, C. D., and Jeanloz, R. W. (1984) *J. Am. Chem. Soc. 106*, 811−813.
23. Griesinger, C., Otting, G., Wüthrich, K., and Ernst, R. R. (1988) *J. Am. Chem. Soc. 110*, 7870−7872.
24. Cieslar, C., Ross, A., Zink, T., and Holak, T. A. (1993) *J. Magn. Res. B 101*, 97−101.
25. Brünger, A. T. (1992) X-PLOR Version 3.1 Manual, Yale University Press, New Haven, CT.
26. Wang, Y., Nip, A. M., and Wishart, D. S. (1997) *J. Biomol. NMR 10*, 373−382.
27. Brünger, A. T., Adams, P. D., Clore, G. M., DeLano, W. L., Gros, P., Grosse-Kunstleve, R. W., Jiang, J.-S., Kuszewski, J., Nilges, M., Pannu, N. S., Read, R. J., Rice, L. M., Simonson, T., and Warren, G. L. (1998) *Acta Crystallogr. D54*, 905−921.
28. Koradi, R., Billeter, M., and Wüthrich, K. (1996) *J. Mol. Graphics 14*, 51−55.
29. Hutchinson, E. G., and Thornton, J. M. (1996) *Protein Sci. 5*, 212−220.

30. Laskowski, R. A., Rullmann, J. A., MacArthur, M. W., Kaptein, R., and Thornton, J. M. (1996) *J. Biomol. NMR 8*, 477−486.
31. Wishart, D. S., and Sykes, B. D. (1994) *Methods Enzymol. 239*, 363−392.
32. Wishart, D. S., Bigam, C. G., Holm, A., Hodges, R. S., and Sykes, B. D. (1995) *J. Biomol. NMR 5*, 67−81.
33. Dyson, H. J., Rance, M., Houghten, R. A., Lerner, R. A., and Wright, P. E. (1988) *J. Mol. Biol. 201*, 161−200.
34. Andersen, N. H., Neidigh, J. W., Harris, S. M., Lee, G. M., Liu, Z., and Tong, H. (1997) *J. Am. Chem. Soc. 119*, 8547−8561.
35. Luckett, S., Santiago Garcia, R., Barker, J. J., Konarev, A. V., Shewry, P. R., Clarke, A. R., and Brady, R. L. (1999) *J. Mol. Biol. 290*, 525−533.
36. Fregeau Gallagher, N. L., Sailer, M., Niemczura, W. P., Nakashima, T. T., Stiles, M. E., and Vederas, J. C. (1997) *Biochemistry 36*, 15062−15072.
37. Aumelas, A., Mangoni, M., Roumestand, C., Chiche, L., Despaux, E., Grassy, G., Calas, B., and Chavanieu, A. (1996) *Eur. J. Biochem. 237*, 575−583.
38. Fahrner, R. L., Dieckmann, T., Harwig, S. S. L., Lehrer, R. I., Eidenberg, D., and Feigon, J. (1996) *Chem. Biol. 3*, 543−550.
39. Kawano, K., Yoneya, T., Miyata, T., Yoshikawa, K., Tokunaga, F., Terada, Y., and Iwanaga, S. (1990) *J. Biol. Chem. 265*, 15365−15367.
40. Tam, J. P., Wu, C., and Yang, J.-L. (2000) *Eur. J. Biochem.* 267, 3289−3300.
41. Tam, J. P., Lu, Y.-A., and Yang, J.-L. (2000) *Biochem. Biophys. Res. Commun.* 267, 783−790.
42. Craik, D. C., Daly, N. L., and Waine, C. (2001) *Toxicon 39*, 43−60.
43. McDonald, N. Q., and Hendrickson, W. A. (1993) *Cell 73*, 421−424.
44. Daly, N. L., Koltay, A., Gustafson, K. R., Boyd, M. R., Casas-Finet, J., and Craik, D. J. (1999) *J. Mol. Biol. 285*, 333−345.
45. Saether, O., Craik, D. J., Campbell, I. D., Sletten, K., Juul, J., and Norman, D. G. (1995) *Biochemistry 34*, 4147−4158.
46. Roumestand, C., Louis, V., Aumelas, A., Grassy, G., Calas, B., and Chavanieu, A. (1998) *FEBS Lett. 421*, 263−267.
47. Qu, X.-D., Harwig, S. S. L., Shafer, W. M., and Lehrer, R. I. (1997) *Infect. Immun. 65*, 636−639.

BI002028T